Applied Physics Letters

RESEARCH ARTICLE | AUGUST 03 2023

Plasmonic metasurface superscatters driven by infrared surface lattice resonances

Seyed M. Sadeghi ; Dustin T. Roberts ; Harrison Knox ; Rithvik R. Gutha

Appl. Phys. Lett. 123, 051702 (2023)
https://doi.org/10.1063/5.0159295

Applied Physics Letters ARTICLE pubs.aip.org/aip/apl

Plasmonic metasurface superscatters driven by infrared surface lattice resonances

Cite as: Appl. Phys. Lett. 123, 051702 (2023); doi: 10.1063/5.0159295
Submitted: 22 May 2023 · Accepted: 20 July 2023 ·
Published Online: 3 August 2023

Seyed M. Sadeghi,[a] Dustin T. Roberts, Harrison Knox, and Rithvik R. Gutha[b]

AFFILIATIONS

Department of Physics and Astronomy, University of Alabama in Huntsville, Huntsville, Alabama 35899, USA

[a]Author to whom correspondence should be addressed: seyed.sadeghi@uah.edu
[b]Current address: Ultraleap, Bristol BS2 0EL, UK.

ABSTRACT

We have demonstrated that plasmonic metasurfaces composed of arrays of Au bowtie nanoantennas can support an infrared bidirectional superscattering state. This state arises when the nanoantennas are coherently coupled together, forming a surface lattice resonance that efficiently guides the infrared range (1–1.6 lm) of incident broadband white light along the plane of the arrays. This process exhibits strong polarization dependence, offering an "OFF" state where a 90 rotation of the incident light polarization effectively suppresses in-plane scattering from all sides. Stokes parameters analysis is used to study the states of polarization of the scattering, demonstrating transformation into a complete depolarized state. The results emphasize the significant influence of the multipolar modes of these nanoantennas on the interference processes associated with such scattering phenomena, and their potential applications in polarization optical switching and unique beamsplitting.

Periodic arrays of metallic nanoantennas can support hybridization of their localized surface plasmon resonances (LSPRs) with the diffraction modes of the arrays, forming surface lattice resonances (SLRs).[1–6] Such resonances offer a coherent process wherein the LSPRs of the nanoantennas are excited in phase.[7] These resonances have been studied under the weak and strong regimes of exciton-SLR coupling[5,8] and are widely used for biological and chemical sensing applications.[9–13] Additionally, owing to their collective nature and sharp spectral features, SLRs have been investigated for excitonic laser systems,[14–16] design of optical filters,[17] study of Rabi splitting, dressed states, and exciton polaritons in monolayers of transition metal dichalcogenides.[18,19] Combination of SLRs and LSPRs is also considered for coherent transport of energy between two very dissimilar quantum dots[20] and the formation of photonic-plasmonic paths for transfer of energy from quantum dots to metallic nanoantennas.[21] In addition, recent reports have considered the impact of SLR in magnetoplasmonic crystals,[22] investigating magnetoplasmonic sensors and beam steering by adding magnetic materials to the structures that support SLRs.[23,24]

Investigation of SLRs based on various types of metallic nanoantennas can offer a wider range of plasmonic metasurfaces with various applications. These nanoantennas include split-ring resonators,[25] nanorods,[26] nanodisks, and dimers.[7,25] Periodic arrays of Bowtie nanoantennas (BTs) and their SLRs have also been utilized to tailor the interaction of light with MoS_2 monolayers.[27,28] Additionally, strong exciton-plasmon interaction supported by BT arrays and their nanoscale gaps have been used to demonstrate anticrossing behaviors and Rabi splitting.[29,30] BTs have also been investigated as receiving and transmitting nanoantennas[31] and for sensor applications.[32] Optimization of nanogaps in BTs for plasmonic enhancement factor has also been studied.[33]

Previous studies on surface lattice resonances (SLRs) in bowtie (BT) arrays have primarily focused on the visible range, around 600 nm.[27–30] In this paper, we investigate a BT array design capable of supporting an infrared SLR [Fig. 1(a)]. We demonstrate that such an SLR can strongly control the in-plane scattering of the array, resulting in an infrared bidirectional superscattering state. This state occurs for a specific polarization of the incident light and enables efficient routing of the infrared (IR) range (1–1.6 lm) of a broadband white light source into the plane of the arrays [Fig. 1(b)]. We show that IR SLRs in BT arrays offer an effective means of switching in-plane scattering. This includes achieving an "OFF" state where in-plane scattering is significantly suppressed in all four directions over a broad range of 0.5–1.6 lm [Fig. 1(c)]. The results highlight the conditions under which a purely linearly polarized incident light becomes depolarized or maintains its polarization state at nearly 100%. These findings

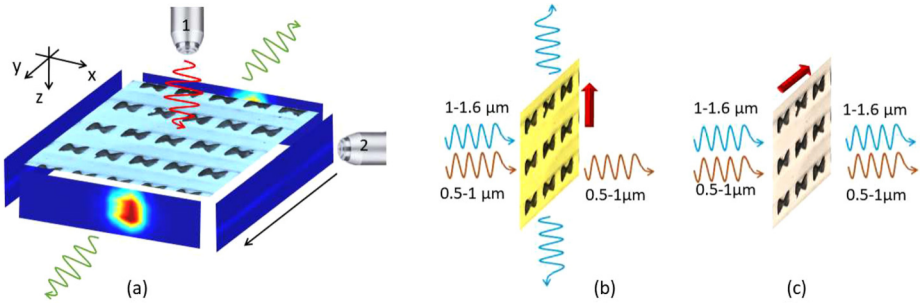

FIG. 1. (a) Schematic of the in-plane scattering measurement setup for BT arrays. (b) and (c) The superscattering and OFF states of these arrays. In (b) and (c), the red arrows refer to the polarization of the incident light along the y- and x-axis, respectively.

provide unique applications of plasmonic metasurfaces, including polarization optical switching and broadband beam splitting.

Note that, recent reports have highlighted the significance of in-plane (side) scattering of single and arrays of nanoantennas as a capable technique to investigate interference processes associated with plasmonic resonances.[34,35] For the case of single nanoantennas, this technique has been used for spin control of quantum emitters[34] and in-plane nanoantennas scattering via multipolar plasmon resonances.[36,37] The in-plane scattering of arrays of V-shaped nanoantennas has revealed the formation and transition between plasmonic bracket supercells.[38] Recent reports have also shown that in-plane scattering can demonstrate interference among the electric dipole, quadrupole, and magnetic dipole moments of a split-ring resonator[37] and can be used for lasing action based on strongly coupled plasmonic nanocavity arrays.[39] Control of such a process via the interference process has been examined in detail via alignment of arrays of dipoles associated with polarization-sensitive apertures in a gold film.[35] In-plane scattering is also uniquely useful for applications of SLRs, including laser systems,[40–42] investigation of diffractive coupling in the plane of the arrays,[43] and control of in-plane scattering using SLRs and localized surface plasmon resonances (LSPRs).[44]

To measure in-plane scattering, we used a setup consisting of an objective to focus the light on the sample (objective 1) and a second objective (objective 2) to collect the light along the edge of the glass substrate supporting the arrays [Fig. 1(a)]. For numerical simulations and mode analysis, we used the finite-difference time-domain (FDTD) technique provided by the Device Multiphysics Simulation Suite of Lumerical (2020a).

E-beam lithography was employed to fabricate bowtie (BT) arrays with lattice constants $a_x = a_y = 1\,1\text{m}$, as highlighted in Fig. S1(a) of the supplementary material, which also includes some details of the fabrication processes. The scanning electron microscopy (SEM) image of the arrays is shown in the inset of Fig. 2(a). The bowties had lengths (L) and widths (W) of approximately 610 and 400 nm, respectively. They were located in regions with $200\,200\,\text{lm}^2$ dimensions at about center of the square glass substrates with 20 mm sides. A transmission setup was used to measure the extinction spectra of these arrays under superstrate conditions of air. The results depicted in Fig. 2(a) illustrate the polarization dependence of the extinction spectra when the incident light was polarized along the x axis (x-pol) and the y axis (y-pol). The solid line corresponds to x-pol, whereas the dashed line represents y-pol. The findings indicate that for x-pol, the spectrum exhibits a prominent peak at around 800 nm, while for y-pol, the spectrum displays peaks at approximately 750 and 1050 nm and a shoulder at 1400 nm.

Figure 2(b) displays the dark field backscattered spectra of the BT array, detected perpendicular to the plane of this array, in the visible range using different microscope objectives. The results demonstrate significant variations attributed to the mode excitation and collection efficiency supported by the objective and dark field filter.[45] The insets in Fig. 2(b) provide microscope images of the BT arrays captured using the 20, 50, and 100 objectives. Previous reports have indi-cated that objectives with smaller magnifications can support a near-normal incidence approach, reducing the effects of retardation fields.[46,47] It should be noted that in this paper, we specifically study the scattering processes that occur perpendicular to the back scattering with long range scanning capability. This offers a less dependency on the collection optics.

The results for in-plane scattering along all four sides of the glass substrate supporting the BT arrays are shown in Figs. 3(a)–3(d).

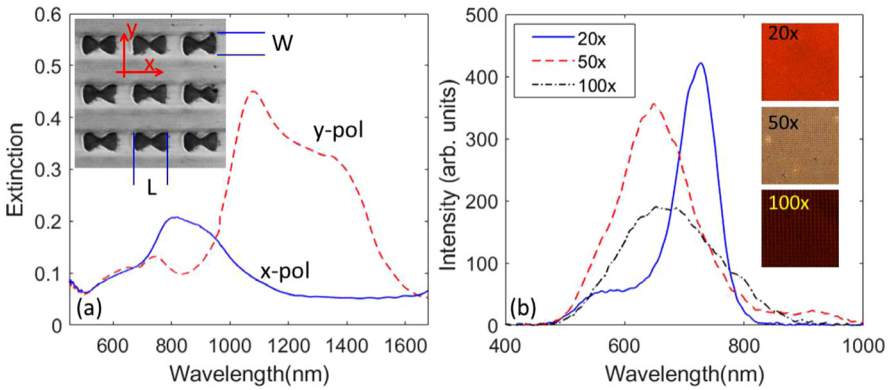

FIG. 2. (a) Extinction spectra of the BT arrays for x-pol (solid line) and y-pol (dashed line). The inset shows the top SEM image wherein L 613 and W 400 nm refer to the width and length of the BT nanoantennas, respectively. (b) Dark field backscattered spectra of the BT arrays with 20 (solid line), 50 (dashed line), and 100 (dashed-dotted line) microscope objective. The insets in (b) show microscope images associated with these objectives.

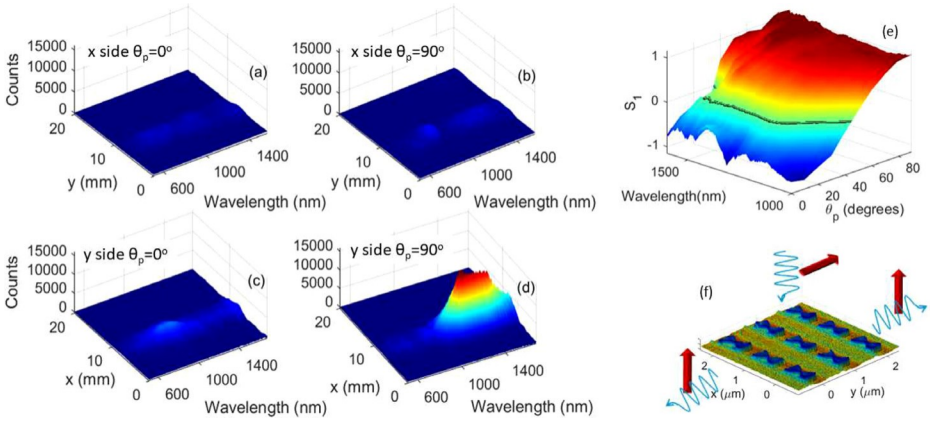

FIG. 3. In-plane scattering of the BT arrays when it is detected along the x axis [(a) and (b)] and y axis [(c) and (d)]. In cases (a) and (c), the incident light has x-pol, and in (b) and (d), it has y-pol. (e) S_1 associated with the scattering along the y-axis in the 1–1.6 lm range. (f) Schematics of the complete polarization reserved scattering process. In (f), the horizontal red arrow shows polarization of the incident light along the y-axis, and the vertical red arrows refer to that of scattered light along the z-axis.

Overall, these figures reveal several interesting features. One is the relatively low scattering counts when the scattering was detected the x-axis of the array for both x-pol and y-pol [Figs. 3(a) and 3(b)]. This is a unique feature compared to arrays of nanorods or V-shaped nanoantennas, where the relative scattering along this axis can be significant.[38,44] The prominent feature, however, is the ultrahigh efficient scattering along the y axis, when the incident light is polarized along the same axis, i.e., y-pol [Fig. 3(d)]. Such a superscattering state occurs in the 1–1.6 lm range, indicating a bidirectional spectral filtering process along the y-axis [Fig. 1(b)]. The significant amount of scattering observed in Fig. 3(d) suggests that this process is a prominent factor in the reduction of the extinction of the BT arrays in the 1–1.6 lm range for transition from the y-pol to x-pol [dashed and solid lines in Fig. 2(a)]. Furthermore, comparing the results in Figs. 3(c) and 3(d) suggests that this superscattering state can be turned off by rotating the polarization of the incident light by 90, i.e., forming the OFF state [Fig. 1(c)]. When in this state, the whole scattering process along all side is suppressed, as indicated by Figs. 3(a) and 3(c). This process offers an infrared switching process. It also suggests a polarization beamsplitting based on metallic metasurfaces. As highlighted in Fig. 3(f), such an application is related to the fact that the scattering process is bidirectional. Figure S2 shows the results confirming that in the OFF state, the extinction of BT arrays is nearly zero for a laser with 1290 nm wavelength, indicating lack of dissipation and scattering.

In order to investigate the polarization states of the in-plane scattering, we analyzed the three components of its Stokes parameters (S_1, S_2, and S_3). Here, S_1 represents the degree of horizontally and vertically polarization, S_2 that of L 6 45, and S_3 the degree of circular polarization of the scattered light. Initially, we examined this for the in-plane scattered light in the 0.5–1 lm range. For the case of 1–1.6 lm IR range, however, we only measured S_1 and S_2 due to limitations of our broadband quarter-wavelength plate. Nevertheless, as demonstrated later, our understanding of the 0.5–1 lm range can be extrapolated to gain insights into the 1–1.6 lm range.

The results in Fig. 4 show variations of normalized Stokes parameters, i.e., $S_1 = S_1/S_0$ (a), $S_2 = S_2/S_0$ (b), and $S_3 = S_3/S_0$ (c) for the scattered light detected along the x-axis ($S_0 = \sqrt{S_1^2 + S_2^2 + S_3^2}$). In Fig. 4, h_p refers to the incident light polarization, with $h_p = 0$ corresponding to x-pol and $h_p = 90$ corresponding to y-pol. The degree of the linearly polarized component, represented by S_1 [Fig. 4(a)], exhibits a clear transition from a horizontally polarized state ($S_1 = 1$) to a vertically polarized case ($S_1 = -1$). However, this transition depends on the wavelength of the incident light. Around 750 nm, this transition occurs at h_p 60, while for 900 nm, it happens at h_p 40. The results for the degree of L þ 45 and L ÿ 45 (S_2) and right and left circularly polarized (S_3) components show some fluctu-ating features [Figs. 4(b) and 4(c)]. These results suggest that the horizontally and vertically polarized components of the in-plane scattering are dominant. Similar results are observed for the scattering along the y axis [Figs. 4(a^0)–4(c^0)]. These findings highlight an important feature, indicating that the scattered light remains predominantly linearly polarized either horizontally or vertically. This suggests that for h_p values where S_1 becomes zero [black lines in Figs. 4(a) and 4(a^0)], the

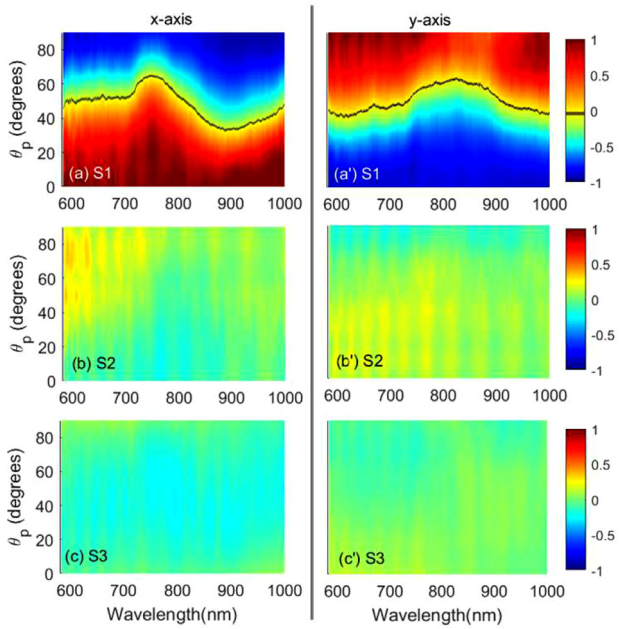

FIG. 4. Stokes parameters for in-plane scattering in the range of 0.6–1 lm. (a)–(c) For scattering detected along the x-axis, and (a^0)–(c^0) scattering detected along the y-axis. The black lines in (a) and (a^0) refer to the cases of $S_1 = 0$.

in-plane scattered light becomes effectively unpolarized. Such a depolarization process can be attributed to the combined effects of BT excitation along the x- and y-axes,[48] and the degree of coupling of different polarization components to the glass substrate. Note that the results for the un-normalized Stokes parameters for the visible range (Fig. S3) and IR range (Fig. S4) show how variations of h_p change the overall intensity of scattered light (S_0).

In the range of 1–1.6 lm, the in-plane scattering along the x axis was found to be insignificant. Similarly, as observed in Fig. 4 for the 0.5–1 lm range, the values of S_2 were also negligible. Figure 3(e) presents the results of S_1 for scattering along the y axis. These findings indicate that for h_p ¼ 90, the in-plane scattering is predominantly vertically polarized, as the value of S_1 is close to unity. As h_p decreases, S_1 gradually declines and reaches zero at certain angles [indicated by the black line in Fig. 3(e)]. The results reveal that for h_p ¼ 30, S_1 approaches zero within the 1.1–1.5 lm range. This suggests that at this angle, a spectrally wide range of unpolarized IR scattering can emerge from the edge of the substrate. As we approach the OFF state with smaller h_p values, the intensity decreases, and S_1 exhibits fluctuating behavior. Fluctuations of S_1 can be associated with the variations in size and shape of nanoantennas, causing random phase and amplitude variations in the scattering, and to wavelength-dependent plasmon modes of the BT nanoantennas.

To investigate the mechanism behind the superscattering state and the OFF state presented in Fig. 3, we studied the plasmonic mode properties and IR SLR in the BT arrays by rotating the sample along the x- and y-axes for x-pol and y-pol, respectively. A significant effect of this rotation is the elimination of the degeneracy of the Rayleigh Anomaly (RA) and the variation of transverse and longitudinal modes of the BTs as the angle of the incident light wavevector is changed. We initially examined the case of x-pol with rotation along the x-axis. In the following analysis, b denotes the angle between the incident light wavevector and the normal of the array [as shown in the inset of Fig. 5(a)]. The results in Fig. 5(a) demonstrate that, for x-pol and rotation along the x-axis, increasing b from 0 (red solid line) to 15 (black dotted line) leads to a spectral transition from a spectrum with a peak at 800 nm and a kink at 918 nm, into another spectrum with a kink at 800 nm and a peak at 918 nm. Beyond 15, the spectra primarily exhibit amplitude suppression (indicated by the solid lines marked with numbers 20 and 25). These results primarily reflect the variations of LSPRs of individual BTs with rotation along the x axis, while the length of the BT remains unchanged.

When we kept the incident light polarization unchanged (x-pol) but rotated the samples along the y-axis, the results changed significantly. Figure 5(b) shows the formation of several peaks, particularly at 806, 940, and 1210 nm when b ¼ 15 (dotted line). As b increases, the overall amplitudes of these peaks decrease. The vivid distinction between the results in Figs. 5(a) and 5(b) can be attributed to the impact of the rotation along the y axis on exciting multipolar plasmonic states of BT for x-pol.

For y-pol and rotation along the y axis, as b increases, the BT arrays show that the peak at about 1100 nm (peak s) starts to reduce in amplitude while the kink at 1300 nm (h) increases [Fig. 5(c)]. For b ¼ 20 and larger, one mostly sees amplitude reduction. For y-pol and rotation along the x-axis, the results become quite unique. As shown in Fig. 5(d), an increase in the value of b allows peak s (circle) and kink h (square) to become closer to each other. For b ¼ 10

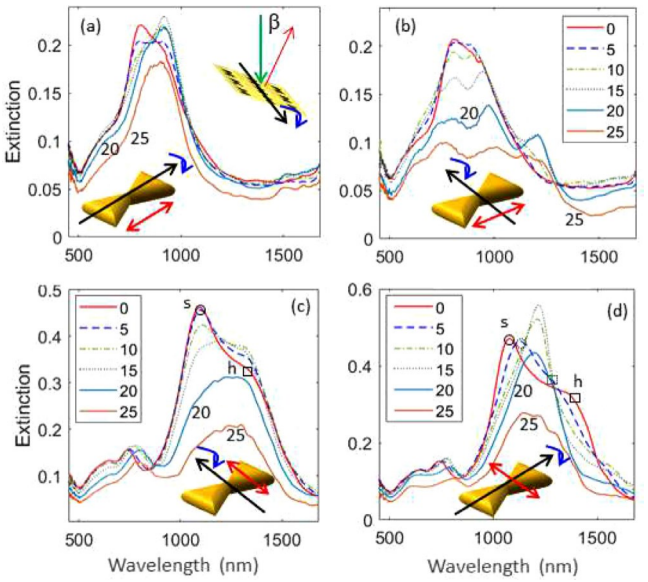

FIG. 5. Variations of the extinction spectra of the BT arrays when they are rotated along the x-axis [(a) and (d)] and the y-axis [(b) and (c)]. In (a) and (b), the incident light has x-pol, and in (c) and (d), it has y-pol. The red solid, blue dashed, green dashed-dotted, and black dotted lines refer to b ¼ 0, 5, 10, and 15, respectively. Lines highlighted with numbers 20 and 25 refer to b ¼ 20 and 25, respectively. The inset in (a) shows the geometry of the rotation wherein the green arrow refers to the incident line direction and the red arrow to the normal of the array. Here, the black one-sided arrows refer to the axes of the rotation, and the red two-side arrows to the polarization directions.

(dashed-dotted line), they merge together, and for b ¼ 15, they overlap well with each other, forming a single, relatively higher amplitude and narrower peak (dotted line). With a further increase in b, the amplitude of this peak reduces as it becomes broader.

To analyze the results in Figs. 5(a)–5(d), it is important to note that the BT arrays have a square lattice, with a_x ¼ a_y ¼ 1 lm. Therefore, they can support two Rayleigh Anomaly (RA) wavelengths: one associated with the substrate, which has a refractive index (n_{sub}) of 1.5 (glass), and the other associated with the superstrate, which has a refractive index (n_{sup}) of 1 (air). As a result, the first-order RA wavelength for the superstrate is 1 lm, while for the substrate, it is 1.5 lm. Therefore, both the substrate and superstrate can support a set of (61, 0) RA modes. The results shown in Fig. 5(d) suggest that peak "s" (circle) is associated with the (61, 0) mode of the superstrate, while kink "h" (square) is related to the (61, 0) mode of the substrate. As the angle b increases, the (þ1, 0) mode of the substrate starts to redshift, while the (ÿ1, 0) mode becomes less visible. Conversely, for the superstrate modes, the (ÿ1, 0) mode blueshifts, while the (þ1, 0) mode is mostly smeared out.[4] The weakness of the RA modes, i.e., (ÿ1, 0) of substrate and (þ1, 0) of the superstrate, can normally be associated with the detuning of the RA wavelength from the LSPRs.[49]

The results represented in Fig. 5(d) point toward the prominent impact of IR SLR on the results shown in Fig. 3, suggesting that the efficient channel of in-plane scattering in the case of the BT arrays is the coherently driven one. To further investigate this, simulations were carried out using the FDTD technique. The incident light was

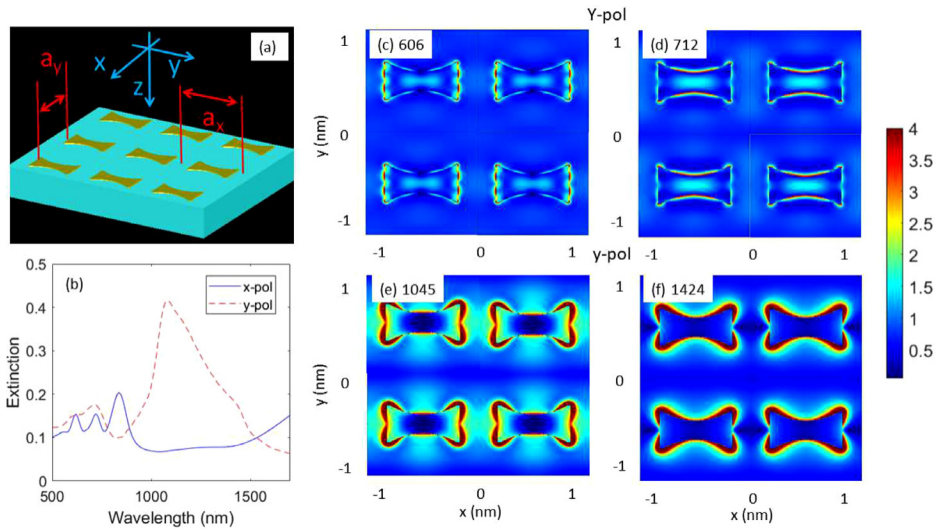

FIG. 6. (a) Simulation structure of the arrays of BTs as in sample A. (b) The spectra of the array for x-pol and y-pol of the BT arrays (sample A). (c)–(f) The spectra for sample field enhancement profiles in the x–y plane for y-pol at 606, 712, 1045, and 1474 nm, respectively.

considered planar, reaching the sample along the z-axis with either x-or y-pol [Fig. 6(a)]. A monitor was placed on the other side of the structure, after the substrate, to find the transmittance (T). The extinction was then calculated using 1ÿT. Numerical studies of the modes of BTs and their arrays have been conducted in the past in the visible range.[27] Here, however, the simulation structures were designed to imitate the BT arrays shown in the inset of Fig. 2(a), which supports IR SLR. Figure 6(b) shows the simulation results for the extinction spectra for x-pol (solid line) and y-pol (dashed line). These results suggest that for x-pol, some small amplitude peaks are generated. For y-pol, however, we see the formation of a dominant broad peak at about 1080 nm and a much smaller amplitude peak at 718 nm [Fig. 6(b)]. This spectrum seems to support a small kink at about 1400 nm.

Mode analysis using FDTD simulations was used to reveal the near-field properties of the BT arrays when the superscattering state occurs. In particular, to study the mode properties associated with the optical features seen in Fig. 6(b) (dashed line), we analyzed the field enhancement mode profiles, defined as the square of the field in the presence of the arrays compared to that in their absence, at different wavelengths for y-pol. The results suggest a transformation in the multipolar modes of the BTs. At 606 nm, we mostly see the modes at the flat edges of these nanoantennas [Fig. 6(c)]. At 712 nm, these modes are smeared out, and the near-field is more enhanced in the middle curved regions [Fig. 6(d)]. However, at 1045 nm, we can see a strong near field and optical field associated with SLR [Fig. 6(e)]. This reveals that the superscattering state can be attributed to the excitation of a transverse dipolar mode in the BTs at around 1 lm, which leads to enhanced scattering and coherent coupling with the neighboring BTs. The wavelengths associated with the SLR can be traced to k_{RA}¼1 lm (RA wavelength), suggesting that it is a SLR peak associated with the orthogonal hybridization of the LSPRs of the BTs with RA in the superstrate. Additionally, at longer wavelengths, the modes are changed, and the optical fields between them disappear [Fig. 6(f)].

Note that the dipolar mode observed in Fig. 6 is highly dependent on the polarization of the incident light. In fact, in the case of x-pol (Fig. S5), the results indicate a transition between multipolar modes, mostly along the curved lengths of the nanoantennas, in the absence of inter-nanoantenna optical coupling. Consequently, the superscattering effect is only observed for y-pol. An important observation from these findings is that in the case of x-pol, the absence of SLRs leads to the system entering an OFF state, where the in-plane scattering along the four sides of the arrays remains relatively low. This process highlights the potential applications of plasmonic metasurfaces in polarization switching and beam splitting, as illustrated in Fig. 1(c).

In conclusion, we have demonstrated the efficient routing of light in the 1–1.6 lm range through coherent excitation of multipolar plasmonic resonances in BT arrays. Our study revealed that BT arrays can exhibit strong in-plane scattering and act as infrared superscatters when they support SLRs in the infrared range. The coherent scattering between the multipolar plasmonic modes of the BTs drives the in-plane scattering for y-pol polarization. Conversely, the absence of SLR formation for x-pol polarization suppresses in-plane scattering, resulting in an OFF state. These findings hold promise for applications in polarization switching, beam splitting, and sensing.

See the supplementary material for details of fabrication and simulation, demonstration of zero dissipation and scattering for the OFF state, results for un-normalized Stokes parameters, and simulation results for x-pol of the BT arrays.

This work was supported by the U.S. National Science Foundation under Grant No. ECCS-1917544.

AUTHOR DECLARATIONS

Conflict of Interest

The authors have no conflicts to disclose.

Author Contributions

Seyed Sadeghi: Conceptualization (lead); Formal analysis (lead); Funding acquisition (lead); Project administration (lead); Writing – original draft (lead). Dustin Roberts: Data curation (equal); Methodology (equal). Harrison Knox: Data curation (equal); Software (equal). Rithvik R. Gutha: Data curation (equal).

DATA AVAILABILITY

The data that support the findings of this study are available within the article.

REFERENCES

[1]V. Kravets, F. Schedin, A. Kabashin, and A. Grigorenko, Opt. Lett. 35, 956 (2010).
[2]S. M. Sadeghi, R. R. Gutha, and W. J. Wing, Opt. Lett. 41, 3367 (2016).
[3]A. Vitrey, L. Aigouy, P. Prieto, J. M. Garcıa-Martın, and M. U. Gonzalez, Nano Lett. 14, 2079 (2014).
[4]R. R. Gutha, S. M. Sadeghi, C. Sharp, and W. J. Wing, J. Phys. D 51, 045305 (2018).
[5]S. R. K. Rodriguez and J. Gomez Rivas, Opt. Express 21, 27411 (2013).
[6]S. M. Sadeghi, W. J. Wing, R. R. Gutha, C. Sharp, and A. Hatef, J. Appl. Phys. 122, 063102 (2017).
[7]V. Kravets, F. Schedin, and A. Grigorenko, Phys. Rev. Lett. 101, 087403 (2008).
[8]A. Tsargorodska, M. L. Cartron, C. Vasilev, G. Kodali, O. A. Mass, J. J. Baumberg, P. L. Dutton, C. N. Hunter, P. Torma, and G. J. Leggett, Nano Lett. 16, 6850 (2016).
[9]R. R. Gutha, S. M. Sadeghi, C. Sharp, and W. J. Wing, Nanotechnology 28, 355504 (2017).
[10]X. Zhang, S. Feng, J. Zhang, T. Zhai, H. Liu, and Z. Pang, Sensors 12, 12082 (2012).
[11]B. D. Thackray, V. G. Kravets, F. Schedin, G. Auton, P. A. Thomas, and A. N. Grigorenko, ACS Photonics 1, 1116 (2014).
[12]B. Auguie and W. L. Barnes, Phys. Rev. Lett. 101, 143902 (2008).
[13]S. Sadeghi, W. Wing, and Q. Campbell, J. Appl. Phys. 119, 244503 (2016).
[14]R. Guo, S. Derom, A. Vakevainen, R. van Dijk-Moes, P. Liljeroth, D. Vanmaekelbergh, and P. Torma, Opt. Express 23, 28206 (2015).
[15]M. Ramezani, G. Lozano, M. A. Verschuuren, and J. G. Rivas, Phys. Rev. B 94, 125406 (2016).
[16]X. Yuan, L. Shi, Q. Wang, C. Chen, X. Liu, L. Sun, B. Zhang, J. Zi, and W. Lu, Opt. Express 22, 23473 (2014).
[17]R. R. Gutha, S. M. Sadeghi, C. Sharp, A. Hatef, and Y. Lin, J. Appl. Phys. 125, 023103 (2019).
[18]W. Liu, B. Lee, C. H. Naylor, H.-S. Ee, J. Park, A. C. Johnson, and R. Agarwal, Nano Lett. 16, 1262 (2016).
[19]S. Wang, S. Li, T. Chervy, A. Shalabney, S. Azzini, E. Orgiu, J. A. Hutchison, C. Genet, P. Samorı, and T. W. Ebbesen, Nano Lett. 16, 4368 (2016).
[20]S. M. Sadeghi, R. R. Gutha, A. Hatef, R. Goul, and J. Z. Wu, ACS Appl. Mater. Interfaces 12, 11913 (2020).
[21]S. M. Sadeghi, R. R. Gutha, C. Sharp, and A. Hatef, J. Phys. D 51, 415301 (2018).
[22]N. Maccaferri, J. Opt. Soc. Am. B 36, E112 (2019).
[23]N. Maccaferri, L. Bergamini, M. Pancaldi, M. K. Schmidt, M. Kataja, S. van Dijken, N. Zabala, J. Aizpurua, and P. Vavassori, Nano Lett. 16, 2533 (2016).
[24]R. M. Rowan-Robinson, J. Hurst, A. Ciuciulkaite, I.-A. Chioar, M. Pohlit, M. Zapata-Herrera, P. Vavassori, A. Dmitriev, P. M. Oppeneer, and V. Kapaklis, Adv. Photonics Res. 2, 2100119 (2021).
[25]R. R. Gutha, S. M. Sadeghi, C. Sharp, and A. Hatef, Nanotechnology 30, 395203 (2019).
[26]G. Vecchi, V. Giannini, and J. Gomez Rivas, Phys. Rev. B 80, 201401 (2009).
[27]B. Lee, J. Park, G. H. Han, H.-S. Ee, C. H. Naylor, W. Liu, A. C. Johnson, and R. Agarwal, Nano Lett. 15, 3646 (2015).
[28]X. Yan and H. Wei, Nanoscale 12, 9708 (2020).
[29]L. Liu, L. Y. Tobing, X. Yu, J. Tong, B. Qiang, A. I. Fernandez-Domınguez, F. J. Garcia-Vidal, D. H. Zhang, Q. J. Wang, and Y. Luo, Adv. Opt. Mater. 8, 1901002 (2020).
[30]W. Liu, Y. Wang, C. H. Naylor, B. Lee, B. Zheng, G. Liu, A. C. Johnson, A. Pan, and R. Agarwal, ACS Photonics 5, 192 (2018).
[31]Z. Fang, L. Fan, C. Lin, D. Zhang, A. J. Meixner, and X. Zhu, Nano Lett. 11, 1676 (2011).
[32]T. Chung, S.-Y. Lee, E. Y. Song, H. Chun, and B. Lee, Sensors 11, 10907 (2011).
[33]S. Dodson, M. Haggui, R. Bachelot, J. Plain, S. Li, and Q. Xiong, J. Phys. Chem. Lett. 4, 496 (2013).
[34]D. Vercruysse, X. Zheng, Y. Sonnefraud, N. Verellen, G. Di Martino, L. Lagae, G. A. Vandenbosch, V. V. Moshchalkov, S. A. Maier, and P. Van Dorpe, ACS Nano 8, 8232 (2014).
[35]J. Lin, J. B. Mueller, Q. Wang, G. Yuan, N. Antoniou, X.-C. Yuan, and F. Capasso, Science 340, 331 (2013).
[36]D. Vercruysse, Y. Sonnefraud, N. Verellen, F. B. Fuchs, G. Di Martino, L. Lagae, V. V. Moshchalkov, S. A. Maier, and P. Van Dorpe, Nano Lett. 13, 3843 (2013).
[37]I. M. Hancu, A. G. Curto, M. Castro-Lopez, M. Kuttge, and N. F. van Hulst, Nano Lett. 14, 166 (2014).
[38]S. M. Sadeghi, D. T. Roberts, R. R. Gutha, S. Allen, and C. Sharp, Phys. Rev. A 106, 063518 (2022).
[39]W. Zhou, M. Dridi, J. Y. Suh, C. H. Kim, D. T. Co, M. R. Wasielewski, G. C. Schatz, T. W. Odom et al., Nat. Nanotechnol. 8, 506 (2013).
[40]J. Guan, M. R. Bourgeois, R. Li, J. Hu, R. D. Schaller, G. C. Schatz, and T. W. Odom, ACS Nano 15, 5567 (2021).
[41]J. Guan, L. K. Sagar, R. Li, D. Wang, G. Bappi, W. Wang, N. Watkins, M. R. Bourgeois, L. Levina, F. Fan et al., ACS Nano 14, 3426 (2020).
[42]A. H. Schokker and A. F. Koenderink, Phys. Rev. B 90, 155452 (2014).
[43]D. Wang, A. Yang, W. Wang, Y. Hua, R. D. Schaller, G. C. Schatz, and T. W. Odom, Nat. Nanotechnol. 12, 889 (2017).
[44]S. M. Sadeghi, R. R. Gutha, S. Ramsay, D. Roberts, and C. Sharp, Mater. Today Nano 18, 100190 (2022).
[45]M. W. Knight, J. Fan, F. Capasso, and N. J. Halas, Opt. Express 18, 2579 (2010).
[46]J. A. Fan, K. Bao, J. B. Lassiter, J. Bao, N. J. Halas, P. Nordlander, and F. Capasso, Nano Lett. 12, 2817 (2012).
[47]L. Jiang, T. Yin, Z. Dong, M. Liao, S. J. Tan, X. M. Goh, D. Allioux, H. Hu, X. Li, J. K. Yang et al., ACS Nano 9, 10039 (2015).
[48]Y. Xu, Z. Wang, and W. Zhang, Opt. Express 28, 24275 (2020).
[49]S. R. K. Rodriguez, A. Abass, B. Maes, O. T. Janssen, G. Vecchi, and J. Gomez Rivas, Phys. Rev. X 1, 021019 (2011).